Antenna Pattern Scattering by Rectangular Cylinders

Hong D. Cheung and Edward V. Jull, *Life Fellow, IEEE*

***Abstract*—The uniform geometrical theory of diffraction (UTD) and the complex source point method are combined to predict two-dimensional (2-D) scattering by rectangular cylinders for E and H-polarized beam sources. Arrays of such beam solutions are also used to model propagation of radio beams into the shadow regions of buildings for local extended sources. Direct numerical verification of the results is obtained for square cylinders of moderate width.**

***Index Terms*—Antenna radiation patterns, cylinders, electromagnetic scattering, geometrical theory of diffraction.**

I. Introduction

THE first of many books by Prof. J. R. Wait includes a wide assortment of scattering and radiation solutions for conducting half planes, wedges, and circular and elliptic cylinders [1], [17]. Sources are usually line sources parallel to the structures and solutions generally are modal expansions, so the numerical results are for cylinder dimensions which are small to moderate in wavelength. Such an analysis has recently been applied to circular cylinders illuminated by beam sources as a model for the prediction of aperture antenna pattern obstruction by cylinders [2]. Here the sources are also beams from a local aperture but the scatterers are rectangular cylinders which can be large in wavelengths. Consequently a very different method of analysis, high frequency diffraction theory in the form of the uniform geometrical theory of diffraction (UTD) [3], is used in combination with the complex source point method [4] to provide a beam source diffraction solution. The results are applicable to the scattering of radio beams by local buildings.

An alternative to UTD in scattering from buildings is the parabolic equation method, a numerical method for a paraxial approximation to the wave equation [5]. It is particularly useful for scattering between buildings along the paraxial direction of the radio beam, a situation where UTD usually encounters difficulty. Special techniques can extend the method outside the paraxial direction [6], but the method is inherently limited in angular range while UTD is not.

Building scattering studies using UTD usually assume plane wave incidence, as appropriate for a distant satellite source [7] or, if the source is local, it is assumed omnidirectional. Often the standard UTD is supplemented with "slope diffraction," based on inclusion of the first derivative of the pattern function, to account for sources of low directivity [8] such as dipoles or small apertures. For more directive local sources, such as large apertures and reflector antennas, neglecting higher order derivatives in the series expansion of the pattern function is generally inadequate. A simple and attractive alternative is conversion of the solution for a local omnidirectional source to a beam source solution. This is done by replacing the source coordinates with complex values which provide a beam of the required directivity and direction [9]. This then represents the near and far field scattered from the building for a local aperture with a single beam and no sidelobes.

In many engineering applications a single beam is sufficient, but often applications require an array of beams arranged in a "Gabor lattice" to represent the field of an aperture with its pattern sidelobes [10]–[12]. In [10] these beam amplitudes are determined approximately from the far-field radiation pattern of the source aperture field. In [11], [12], they are determined directly from the source aperture distribution and then the field at any range is represented to any accuracy desired if enough beams are used. If in addition, the beam basis solutions are from an exact [2], [13] or highly accurate solution for an omnidirectional source near the scatterer, then scattering by the entire local incident field can be found to a similar accuracy. This approach is used here, but for convenience and efficiency only the most significant beams in the array are chosen. Investigations of various beam arrangements are in [11], [12] and justification for the arrangement here is in [13].

The analysis and numerical examples here are limited to square cylinders to take advantage of the simplifications of symmetry, but can be extended to any polygonal cylinder. Other factors affecting our choice of numerical examples are the relative dimensions of source, scatterer and their separation. Source directivity is a particularly significant factor when these dimensions are comparable and not very large in wavelengths. Small obstacles may lie in a region of the source beam where the field is essentially uniform. Large obstacles, such as buildings, can behave as reflecting planes or semiinfinite wedges for local sources. Consequently our examples are limited to scattering by cylinders comparable in dimensions of a few wavelengths to the distance and width of the local source apertures. This means that interaction between the edges can be significant, particularly for H-polarization. It also means that the rectangular cylinders are small enough to permit direct numerical verification of our expressions, which can then be used for much larger structures.

II. Analysis

A. Complex Source Point Beams

Assigning complex values to the coordinates of an omnidirectional source can produce a beam, which is paraxially Gaussian [4]. The far field of a two-dimensional (2-D) line source at

Manuscript received September 6, 1999; revised March 14, 2000.

The authors are with the Department of Electrical and Computer Engineering, University of British Columbia, Vancouver, BC V6T 1Z4, Canada.

Publisher Item Identifier S 0018-926X(00)09832-X.

r_o, θ_o from the origin of coordinates with a beam parameter $\overrightarrow{b} = (b, \beta)$ at any observation point r, θ may be written as

$$E_z^i = \sqrt{\frac{\pi}{2}} e^{-j\pi/4} H_o^{(2)}(kR_s) \approx \frac{e^{-jkR_s}}{\sqrt{kR_s}}, \quad |kR_s| \gg 1 \quad (1)$$

where R_s is the distance between the observation point and the complex source position

$$R_s = \sqrt{r^2 + r_s^2 - 2rr_s\cos(\theta - \theta_s)}. \quad (2)$$

Here $\overrightarrow{r}_s = (r_s, \theta_s)$ is the complex source position, which is related to the real coordinates and the beam parameters by

$$r_s = \sqrt{r_o^2 - 2jbr_o\cos(\beta - \theta_o) - b^2}, \quad \mathrm{Re}(r_s) > 0$$
$$\theta_s = \cos^{-1}\left(\frac{r_o\cos\theta_o - jb\cos\beta}{r_s}\right). \quad (3)$$

The beam width and direction are defined by b and β, respectively. In the far-field limit ($r \gg r_o$) (1) represents an omnidirectional cylindrical wave modulated by a beam pattern $e^{kb\cos(\theta-\beta)}$ with its maximum in direction $\theta = \beta$, its minimum in the direction $\theta = \pi + \beta$ and its half power beamwidth

$$HPBW = 2\cos^{-1}(1 - \ln 2/(2kb)). \quad (4)$$

Rays from a single complex source point generate a single beam without radiation pattern sidelobes. However, more realistic antenna radiation patterns having sidelobes must be represented by radiation from more than one beam. It has already been shown that antenna patterns with sidelobes can be synthesized from arrays of Gaussian beams [11], [12] and this representation applies to both near and far radiation patterns of the aperture. The radiation field of an aperture can be well represented by an array of $2M + 1$ parallel beams $w(x)$ spaced $L = \lambda/2$ along the x-axis [13]. These beams are all in the direction $\beta = 3\pi/2$ and have widths $kb = \pi/2$. Thus the aperture field is

$$E_z(x, 0) = \sum_{m=-M}^{M} A_m w(x - mL), \quad (5)$$

where the amplitude coefficients A_m are obtained by convolving the desired aperture distribution with a biorthogonal function as in [11]. The field in $y > 0$ can then be written as

$$E_z(x, y) = \sum_{m=-M}^{M} A_m B_m(x, y), \quad (6)$$

where B_m are the elementary beam solutions.

This particular arrangement includes the radiating near fields of the aperture, but not the evanescent fields. Thus it is valid for the scattered far fields of obstacles within very few wavelengths of the aperture. Real coordinates $r_{o[m]}$, $\theta_{o[m]}$ of each of the sources are replaced by complex coordinates $r_{s[m]}$, $\theta_{s[m]}$ as in (3) to provide the beam fields.

B. Diffraction by a Conducting Square Cylinder

1) E-Polarization: Fig. 1(a), (b), and (c) show a square conducting cylinder illuminated by a linear array of complex sources with the angle of the array inclined at $\theta_o = 135°$ off a face of the cylinder. With a square cylinder symmetry allows consideration of the scattered far field in only the half-space $-45° < \theta < 135°$. For normal incidence on a face, as in Fig. 1(d), we need to determine the scattered far field only in $-90° < \theta < 90°$.

The total scattered far field will be a superposition of the scattered fields of each complex source point beam in the array by each of the four edges and surfaces of the cylinder. An elementary UTD beam solution for scattering by each source by a single wedge has been given [9]. For the basis elements $B_m(x, y)$ in (6), we use the solution for the total field at r, θ in cylindrical coordinates due to the beam source at $r_{o[m]}$, $\theta_{o[m]}$ and parallel to the edge with beam parameters b_o, β_o

$$B_m = E_{z[m]}^i u\left(\theta_{siB[m]} - \pi + \theta\right) + E_{z[m]}^{rAB} u\left(\theta_{srB[m]} - \pi + \theta\right) \cdot u\left(\theta_{srA[m]} - \theta\right) + E_{z[m]}^d. \quad (7)$$

Here $E_{z[m]}^i$, $E_{z[m]}^{rAB}$, and $E_{z[m]}^d$ are, respectively, the incident field, the field reflected from plane AB, and the total diffracted fields from the edges A, B and C. $u(z)$ is a unit step function. $\theta_{siB[m]}$ and $\theta_{srB[m]}$ are the shadow and the reflection boundaries due to edge B measured clockwise from plane AB and $\theta_{srA[m]}$ is the reflection boundary due to edge A measured counterclockwise from plane AB. The incident far field with coordinates referred to edge A [see Fig. 1(a)] is

$$E_{z[m]}^i = \frac{e^{-jk\left[r_A - r_{sA[m]}\cos\left(\theta_A - \theta_{sA[m]}\right)\right]}}{\sqrt{kr_A}}. \quad (8)$$

The shadow boundary for this incident field $E_{z[m]}^i$ due to the edge B is

$$\theta_{siB[m]} = \pi + \theta_{oB[m]} \mp \cos^{-1}\left(\frac{\mathrm{Re}\left(r_{sB[m]}\right)}{r_{oB[m]}}\right)$$
$$\beta_o^B \gtrless \pi + \theta_{oB[m]}. \quad (9)$$

The far field reflected from the plane AB is

$$E_{z[m]}^{rAB} = -\frac{e^{-jk\left[r_A - r_{sA[m]}\cos\left(\theta_A + \theta_{sA[m]}\right)\right]}}{\sqrt{kr_A}}. \quad (10)$$

The reflection boundaries for reflected field $E_{z[m]}^{rAB}$ due to edges A and B are

$$\theta_{srA[m]} = \pi - \theta_{oA[m]} \pm \cos^{-1}\left(\frac{\mathrm{Re}\left(r_{sA[m]}\right)}{r_{oA[m]}}\right)$$
$$\beta_o^A \gtrless \pi + \theta_{oA[m]}$$
$$\theta_{srB[m]} = \pi - \theta_{oB[m]} \pm \cos^{-1}\left(\frac{\mathrm{Re}\left(r_{sB[m]}\right)}{r_{oB[m]}}\right)$$
$$\beta_o^B \gtrless \pi + \theta_{oB[m]}. \quad (11)$$

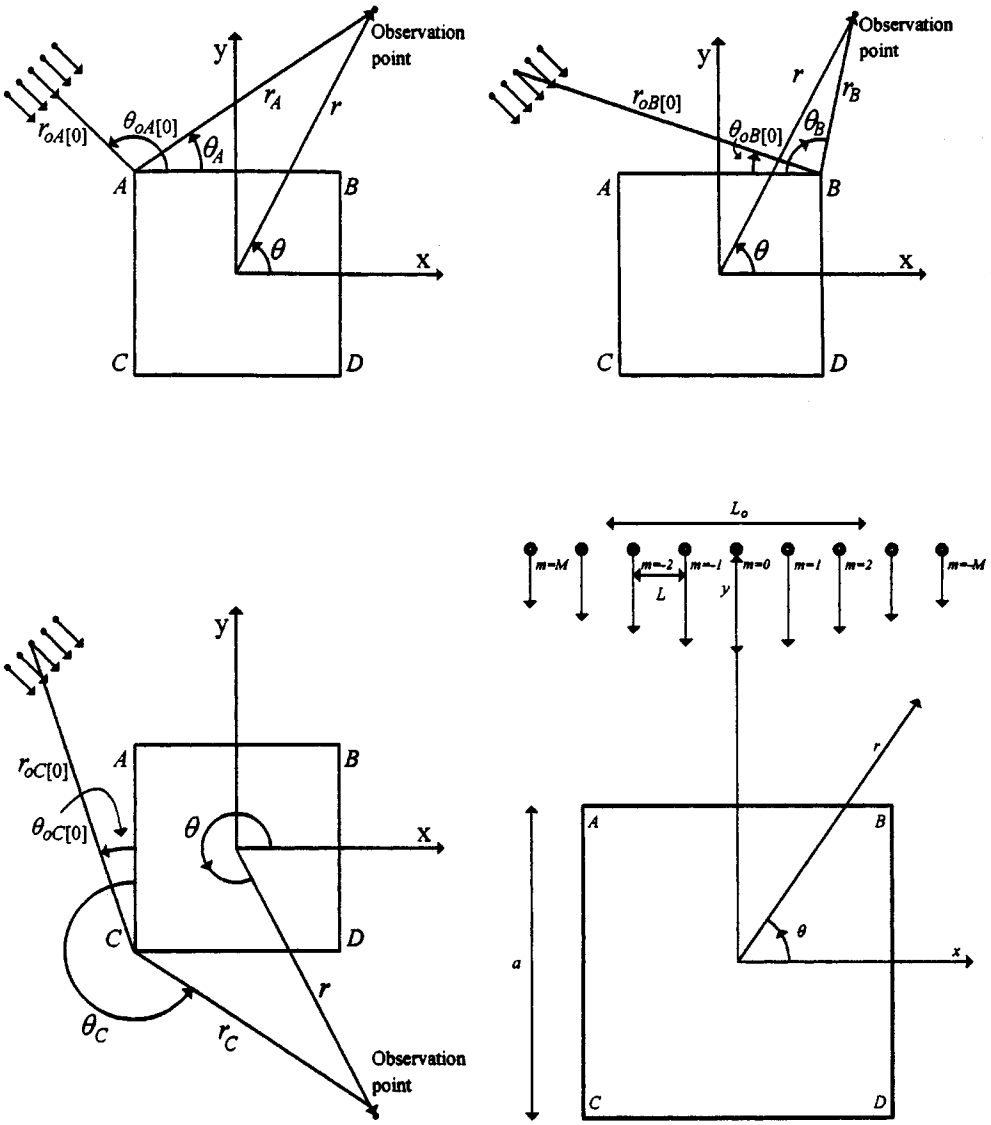

Fig. 1. Geometry of an array of complex source beams for diffraction by a conducting square cylinder. (a), (b), (c) Symmetric incidence on a corner. (d) Normal incidence on a face..

The field diffracted by edges A, B, and C contribute to the total diffracted field $E^d_{z[m]}$. The general expression for the field diffracted by edges A, B, and C is given by

$$E^{d(A,B,C)}_{z[m]} = \frac{e^{-jk\left(r_{(A,B,C)}+r_{s(A,B,C)[m]}\right)}}{\sqrt{kr_{(A,B,C)}}\sqrt{kr_{s(A,B,C)[m]}}} \cdot D\left(\theta_{s(A,B,C)[m]}, \theta_{(A,B,C)}, r_{s(A,B,C)[m]}\right) \tag{12}$$

with a uniform diffraction coefficient $D(\theta_{s(A,B,C)[m]}, \theta_{(A,B,C)}, r_{s(A,B,C)[m]})$ for CSP beam incidence defined as in [9]. $r_{(A,B,C)}$, $r_{s(A,B,C)[m]}$, $\theta_{(A,B,C)}$, and $\theta_{s(A,B,C)[m]}$ replace r, r_s, θ, and θ_s for edges A, B, and C, respectively, and $r_{s(A,B,C)[m]}$, and $\theta_{s(A,B,C)[m]}$ are calculated as in (3). with $r_{o(A,B,C)[m]}$, $\theta_{o(A,B,C)[m]}$, and $\beta_o^{(A,B,C)}$ replacing r_o, θ_o and β. Now the diffracted field by a complex line source can be written as

$$E^d_{z[m]} = \begin{cases} E^{dA}_{z[m]} + E^{dB}_{z[m]} + E^{dC}_{z[m]}, & \pi/2 \le \theta < 3\pi/4 \\ E^{dA}_{z[m]} + E^{dB}_{z[m]}, & 0 \le \theta < \pi/2 \\ E^{dB}_{z[m]} + E^{dC}_{z[m]}, & -\pi/4 \le \theta < 0. \end{cases} \tag{13}$$

In above equations, $r_{(A,B,C)}$, $r_{o(A,B,C)[m]}$ and $r_{s(A,B,C)[m]}$, are the distances of the observation point P, the real source point and the complex source point to the edges A, B and C respectively. θ_A, $\theta_{oA[m]}$, $\theta_{sA[m]}$, and β_o^A are the directions of r_A, $r_{oA[m]}r_{sA[m]}$ and the beam vector $j\vec{b}_o$ measured counter-clockwise from plane AB or the x axis [see Fig. 1(a)]. Similarly θ_B, $\theta_{oB[m]}$, $\theta_{sB[m]}$, and β_o^B are the directions of r_B, $r_{oB[m]}r_{sB[m]}$ and the beam vector $j\vec{b}_o$

measured clockwise from plane AB or the $-x$ axis [see Fig. 1(b)], θ_C, $\theta_{oC[m]}$, $\theta_{sC[m]}$, and β_o^C are the directions of r_C, $r_{oC[m]}r_{sC[m]}$ and the beam vector $j\vec{b}_o$ measured clockwise from plane AC or the y axis [see Fig. 1(c)]. Beam sources normally incident upon the rectangular cylinder plane AB can be treated similarly as above. Then

$$B_m = E^i_{z[m]} u\left(\theta_{siB[m]} - \pi + \theta\right) + E^{rAB}_{z[m]} u\left(\theta_{srB[m]} - \pi + \theta\right) + E^d_{z[m]} \quad (14)$$

and

$$E^d_{z[m]} = E^{dA}_{z[m]} + E^{dB}_{z[m]}, \quad 0 < \theta \le \pi/2, \qquad E^{dB}_{z[m]}, \quad -\pi/2 < \theta \le 0. \quad (15)$$

2) H-Polarization: For H polarization, H replaces E in the above expressions, the $(-)$ sign in the nonexponential part of the reflected wave in (10) becomes $(+)$ and the diffraction coefficient $D(\theta_{s(A,B,C)[m]}, \theta_{(A,B,C)}, r_{s(A,B,C)[m]})$is multiplied by a factor $(-1)^{i+1}$. This noninteraction solution alone is generally inadequate for H polarization. In order to improve the accuracy it is necessary to include also first order interaction between adjacent edges. In the cases discussed there are six more terms to be added for inclined incidence on edge A and four other terms added for normal incidence on side AB. The singly diffracted field of an edge in the direction of an adjacent edge is replaced by the field of a line source of equal amplitude located at the edge. For example, the doubly diffracted field from edge B is produced by the singly diffracted field from edge A in the $\theta_A = 0$ direction. This can be written as

$$H^{dAB}_{z[m]} = \frac{e^{-jk\left(r_{sA[m]}+a+r_B\right)}}{\sqrt{kr_{sA[m]}}\sqrt{ka}\sqrt{kr_B}} D\left(\theta_{sA[m]}, 0, L_{AB[m]}\right) \cdot D\left(0, \theta_B, r_{sB[m]}\right) \quad (16)$$

where a is the width of the square cylinder and $L_{AB[m]}$ is the distance parameter

$$L_{AB[m]} = \frac{a r_{sA[m]}}{a + r_{sA[m]}}. \quad (17)$$

III. Numerical Results

A. E-Polarization

Fig. 2 shows the total far-field patterns at r, θ for a single beam source $(m = 0)$ with $kb_0 = 0.8$, and $\beta_0^A = 7\pi/4$ radians parallel to and at $kr_{oA[0]} = 16$, $\theta_{oA[0]} = 135°$ from the upper left edge of a square cylinder of width 2λ for E polarization [Fig. 1(a)]. The solid curve is the singly diffracted field calculated with basis element B_o calculated from (7) and with $A_o = 1$. The dotted curves in Fig. 2 are from a calculation by the moment method with a point-matching technique [14]. For an omnidirectional source the results essentially coincide, but with stronger edge illumination of edges A, B and C occurring for a more directive source differences between the results appear in Fig. 2(b) in the directions around $\theta = 0, 90°$ because edge interaction is omitted from the UTD result. It is evident that this is a minor omission with E-polarization for cylinders of this dimension.

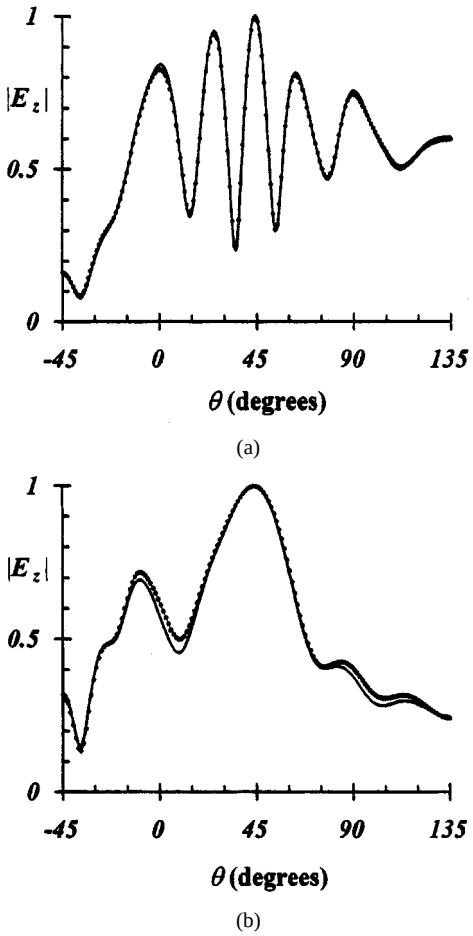

Fig. 2. E-polarized far field of a square cylinder for a single beam source $(kr_o = 16, \theta_o = 3\pi/4, a = 2\lambda)$, (a) $kb = 0$, (b) $kb = 8$, UTD solution (single diffraction), moment method.

Pattern oscillations in these results arise from interference between direct, reflected and diffracted fields. These are very prominent when the source is omnidirectional $(kb = 0)$ but suppressed with increasing directivity outside the reflection region because edges B and C are more weakly illuminated. However the minor lobe in the shadow region (at $\theta = -45°$) increases with increasing directivity for these parameters because more of the incident field is intercepted. Note that for $kb = 8$, the half power beamwidth is about 34°, so the square cylinder of side 2λ is just inside the angle subtended by the half power points of the far-field pattern. The lobes at $\theta = 25°$ and $45°$ in Fig. 2(a) occur at shadow boundaries at edges B and A, respectively. A more directive beam source acts like an aperture distribution with rays emerging from it which are more nearly parallel, so that as beam directivity increases the two reflection boundary lobes merge at $\theta = 45°$, [Fig. 2(b)].

Fig. 3 shows similar results for a larger cylinder with side $a = 5\lambda$. The several pattern lobes in the reflection region $45° < \theta < 135°$ for an omnidirectional source coalesce with even moderate source directivity into a single reflection lobe with its peak at about $\theta = 30°$. If we increase the size of the square cylinder to $a = 25\lambda$, the total field in $0 < \theta < 135°$ resembles that for a single beam source incident on a right angled wedge.

In Fig. 4, the total far field is shown for a single beam source normally incident upon the face of width $a = 2\lambda$ of a square

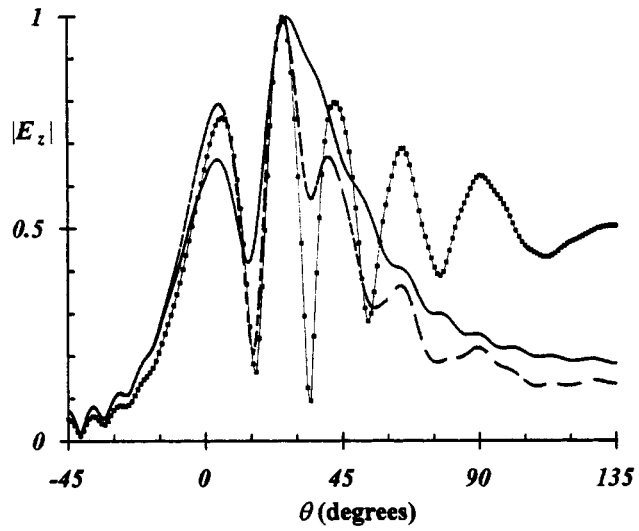

Fig. 3. E-polarized far field (UTD single diffraction) of a squared cylinder for a single beam source. ($kr_o = 16$, $\theta_o = 3\pi/4$, $a = 5\lambda$), $kb = 4$, $kb = 2$, $kb = 0$.

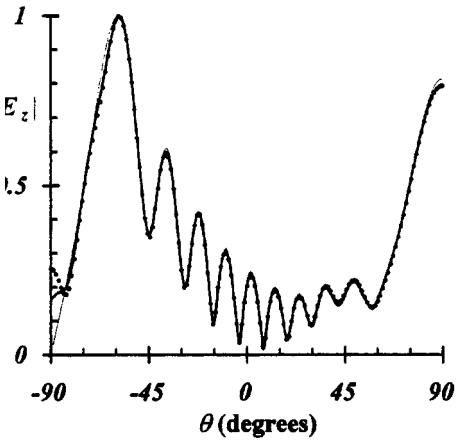

(a)

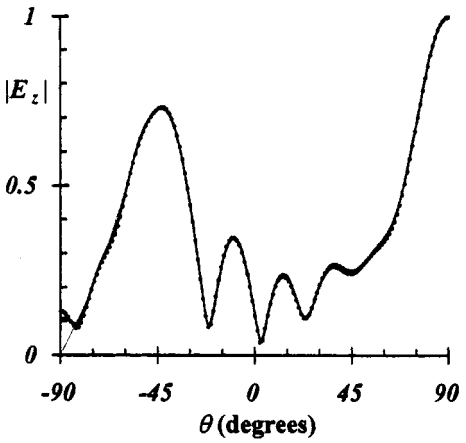

(b)

Fig. 4. E-polarized far field of a square cylinder for a single beam source $kb = 2$ at a distance r_o above the upper surface. ($\theta_o = \pi/2$, $a = 2\lambda$), (a) $kr_o = 32$, (b) $kr_o = 16$, UTD solution (single+double diffraction), UTD single diffraction only, moment method.

cylinder as in Fig. 1(d). Both single and double (slope) diffraction are included in the UTD solution and good agreement with

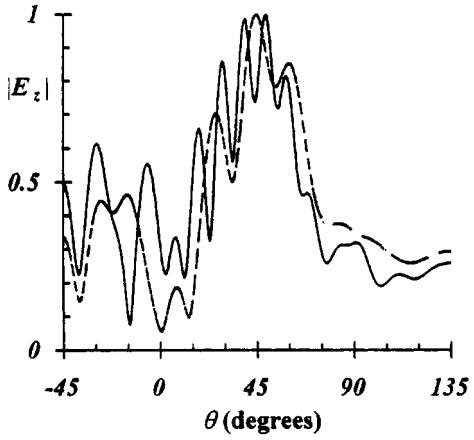

(a)

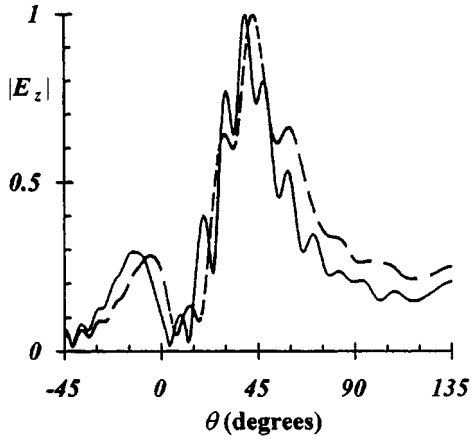

(b)

Fig. 5. E-polarized far field (UTD single diffraction only) for a uniform aperture distribution at a distance of r_o from the edge of a perfectly conducting square cylinder. ($\theta_o = 3\pi/4$, $M = 2$, $L_o = 2.5\lambda$, $L = \lambda/2$), (a) $a = 2\lambda$, (b) $a = 5\lambda$, $kr_o = 32$, $kr_o = 16$.

the moment method values is evident everywhere except in the shadow region ($\theta = -90°$). Indeed that is evidently the only region where double diffraction is needed for these parameters. Double (slope) diffraction is almost adequate in accounting for edge interaction here for the shorter range $kr_o = 16$ but fails for larger separations ($kr_o = 32$) where source, scattering edges and field point are more aligned. This is well known as a difficult arrangement in UTD scattering calculations for which other techniques have been developed [15], [16].

Fig. 5 compares the total far-field patterns at r, θ for a uniform aperture distribution at $kr_{o[0]} = 16$ and 32 from edge A of a square cylinder of side 2λ and 5λ calculated with basis elements $B_m(r, \theta)$ from (7). The angle of incidence $\theta_{oA[0]}$ of the axis of the aperture with respect to edge α is 135°. The aperture size in wavelengths is $L_o = 2.5\lambda$, and it is simulated by $5(M = 2)$ complex source parallel beams spaced $L = \lambda/2$. The central beam is directed at the edge A ($\beta_0^A = 7\pi/4$) and each beam directivity is $kb_o = \pi/2$. In each case, for cylinders of side $a = 2\lambda$ [Fig. 5(a)] and $a = 5\lambda$ [Fig. 5(b)], more pattern oscillations appear for the more distant source due to stronger interference between direct, reflected and diffracted fields. With the same distance from the edge to the aperture, the far-field patterns of the large cylinder show a sharper peak around $\theta = 45°$,

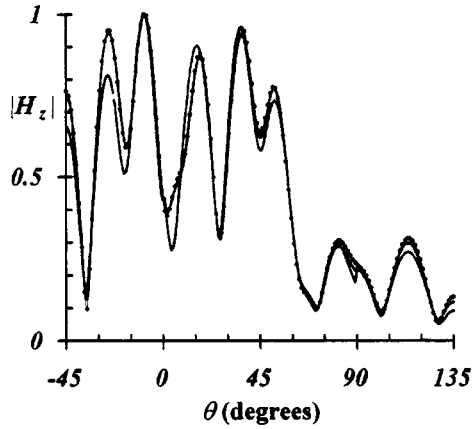

Fig. 6. H-polarized far field of a square cylinder for a single beam source ($kr_o = 16,\ \theta_o = 3\pi/4,\ a = 2\lambda,\ kb = 2$), UTD solution (single diffraction), (single+double diffraction), moment method.

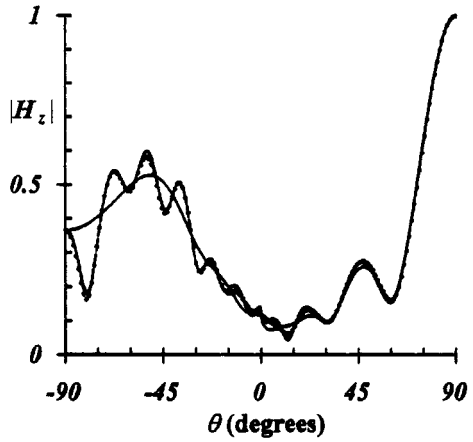

Fig. 8. H-polarized far field of a squared cylinder for a single beam source ($kr_o = 16,\ \theta_o = \pi/2,\ a = 2\lambda,\ , kb = 2$), UTD solution (single diffraction), (single+double diffraction), moment method.

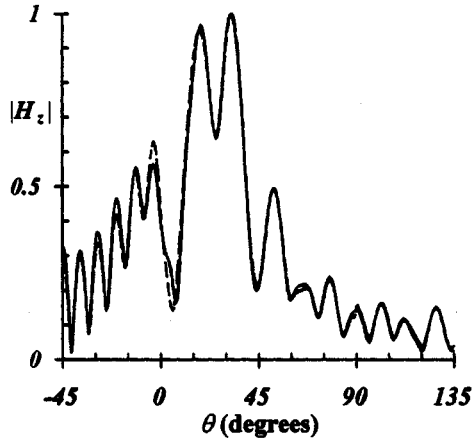

Fig. 7. H-polarized far field of a square cylinder for a single beam source ($kr_o = 16,\ \theta_o = 3\pi/4,\ a = 5\lambda,\ kb = 2$), UTD solution (single diffraction), (single + double diffraction.

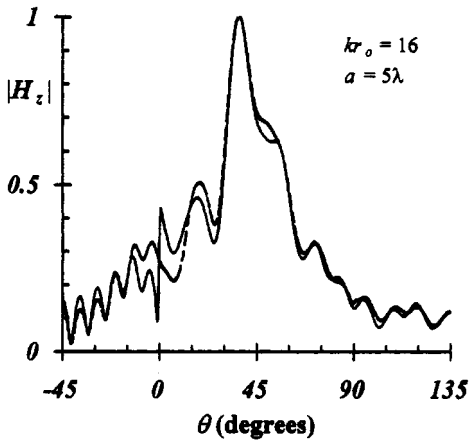

(a)

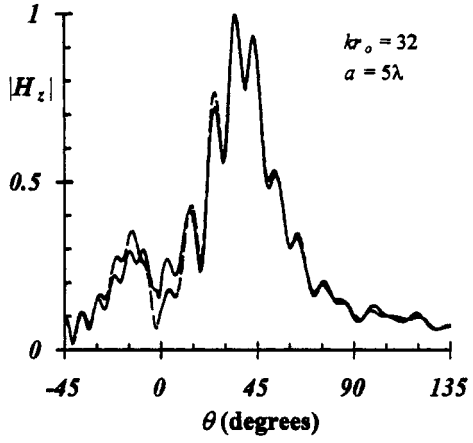

(b)

Fig. 9. H-polarized far-field diffraction patterns of a uniform aperture distribution at a distance of r_o from the edge of a perfectly conducting square cylinder. ($\theta_o = 3\pi/4,\ M = 2,\ L_o = 2.5\lambda,\ L = \lambda/2$), single diffracted field only, single + double diffracted field.

corresponding to the position of the reflection boundary of edge A, and less penetration into the shadow region $\theta < 0$. Single diffraction alone is required in Fig. 5 since it is known from Fig. 2 that it yields reliable results even for $a = 2\lambda$ for the relatively low directivity beams comprising the array.

B. H-Polarization

Figs. 6 and 7 show the total far-field patterns at $r,\ \theta$ for a single beam source ($m = 0$) with $kb_0 = 2$ and 4, $\beta_0^A = 7\pi/4$ radians, parallel to and at $kr_{oA[0]} = 16,\ \theta_{oA[0]} = 135°$ from the upper left edge of a square cylinder of sides 2λ and 5λ for H polarization. The dashed curves include only the singly diffracted fields and the solid curves include also first order interaction between adjacent edges of the square cylinder. Comparison with the numerical solution in Fig. 6 (dotted curves) shows that inclusion of this double diffraction is essential for accuracy with the smaller cylinder. The discontinuity in the single diffraction calculation along the diffraction boundaries such at $\theta = 0°$ and $90°$ is reduced by including the doubly diffraction field. Fig. 7 shows that double diffraction also improves the accuracy for the larger

cylinder, particularly in the region of these diffraction boundaries. In another study [7] H-polarized double diffraction is included for a much larger rectangular structure.

The importance of H-polarized double diffraction in the lateral and shadow regions of the scattering pattern, but much less in the reflection region, is very clearly shown in the results for normal incidence of Fig. 8. The backscattered doubly diffracted fields are relatively insignificant even for small cylinders and directive sources (as shown by other results), but not the forward scattered fields and this is verified by the numerical solution. Notice that the discontinuity at $\theta = 0°$ decreases with increasing beam directivity and that the total field in the forward direction ($\theta = -90°$) is almost entirely contributed by single diffraction, in contrast to the situation for ε-polarization. Similar results are observed for a more distant source incident upon on the cylinder.

Fig. 9 shows the far scattered field patterns at r, θ for the beam axis of a uniform aperture distribution directed at edge α of a square cylinder of side 5λ. The aperture is located at distances from the edge A of $kr_{oA[0]} = 16$ and 32 and the angle of incidence $\theta_{oA[0]}$ of the beam axis of the aperture distribution with respect to side AB is $135°$. The aperture width is $L_o = 2.5\lambda$. All the line source beams are spaced $L = \lambda/2$ apart with axes normal to the aperture ($\beta_0^A = 7\pi/4$) with directivity $kb_o = \pi/2$. The solid curves show singly diffracted fields. The dashed curves singly plus doubly diffracted fields. The latter are now somewhat more necessary for accuracy in the lateral and forward regions of the pattern than they were for single beam incidence. Also double diffraction removes a pattern discontinuity at $\theta = 0°$ where edges A, B and the field point are aligned. This discontinuity is much more prominent in the singly diffracted field pattern at the shorter range $(kr_o = 16)$ than the longer $(kr_o = 32)$, the opposite of the situation in the shadow region of Fig. 4 for E-polarization. Corresponding results for smaller $(a = 2\lambda)$ cylinders show much more field penetration into the shadow regions of the cylinder than in Fig. 9, particularly for the larger range $kr_o = 32$.

IV. Conclusion

The complex source point method and the UTD can be combined efficiently to predict radio beam propagation around local conducting cylinders. If a single beam inadequately represents the near field of an antenna aperture we may use an array of complex source point beams in a Gabor lattice to represent the source field to any desired degree of accuracy. Although the numerical results here are for square cylinders the procedure can be extended to any polygonal cylinder. While the cylinder walls have been assumed perfectly conducting here and in [7] we may also use impedance boundary conditions appropriate to building surfaces. Our preliminary results for this indicate that it is mainly the amplitude, rather than the structure, of the scattered field which is affected. Aperture antenna pattern blockage by local buildings may then be predicted in this way with more accuracy than is available with the alternative parabolic equation method [5], which seems most suited for larger domains and for propagation over nearly aligned building edges.

The numerical results shown here provide insight into appropriate polarization and beam directivities for effective penetration into the shadow regions of local rectangular obstacles. H-polarization is found to be more effective in this regard and greater directivity can enhance it provided illumination of the diffracting edges adjacent to the shadow region is maintained. This of course is directly related to the observation that double diffraction is significant for H-polarization field calculations in the lateral and shadow regions of the cylinders, while for E-polarization single diffraction is generally adequate, even for relatively, small cylinders, except when source, diffracting edges and field point are aligned. The numerical results also confirm the observation [13] that while single beams may represent sources if the scatterers are sufficiently small and distant, larger and nearer scatterers require source representation by a beam array.

References

[1] J. R. Wait, *Electromagnetic Radiation from Cylindrical Structures*. New York: Pergamon, 1959.

[2] H. D. Cheung and E. V. Jull, "Scattering of antenna beams by local cylinders," *J. Electromagn. Waves Applicat.*, vol. 13, pp. 1315–1331, 1999.

[3] R. G. Kouyoumjian and P. H. Pathak, "A uniform geometrical theory of diffraction for an edge in a perfectly conducting surface," *Proc. IEEE*, vol. 62, pp. 1448–1461, Nov. 1974.

[4] G. A. Deschamps, "Gaussian beam as a bundle of complex rays," *Electron. Lett.*, vol. 7, pp. 684–685, 1971.

[5] M. F. Levy, "Diffraction studies in urban environment with parabolic equation method," *Electron. Lett.*, vol. 28, pp. 1491–1492, 1992.

[6] ——, "Parabolic wave equation techniques for radiowave propagation," URSI Radio Sci. Bull., no. 282, Sept. 1997.

[7] P. A. Tirka, C. M. Wangsvick, and C. A. Balanis, "Propagation model for building blockage in satellite mobile communications systems," *IEEE Trans. Antennas Propagat.*, vol. 46, pp. 991–997, July 1998.

[8] R. G. Kouyoumjian and P. H. Pathak, "A uniform GTD approach to EM scattering and radiation," in *Low and High Frequency Asymptotics*, V. K. Varadan and V. V. Varadan, Eds. Amsterdam, The Netherlands: Elsevier, 1986, ch. 3, pp. 266–333.

[9] G. A. Suedan and E. V. Jull, "Beam diffraction by half planes and wedges: Uniform and asymptotic solutions," *J. Electromagn. Waves Applicat.*, vol. 3, no. 1, pp. 17–26, 1989.

[10] R. J. Burkholder and P. H. Pathak, "Analysis of EM penetration into and scattering by electrically large open waveguide cavities using Gaussian beam shooting," *Proc. IEEE*, vol. 79, pp. 1401–1412, Oct. 1991.

[11] P. D. Einziger, S. Raz, and M. Shapira, "Gabor representation and aperture theory," *J. Opt. Soc. Amer. A*, vol. 3, no. 4, pp. 508–522, Apr. 1986.

[12] J. J. Maciel and L. B. Felsen, "Systematic study of fields due to extended sources by Gaussian beam discretization," *IEEE Trans. Antennas Propagat.*, vol. 37, pp. 884–892, July 1989.

[13] H. D. Cheung and E. V. Jull, "Two-dimensional diffraction by half-planes and wide slits near radiating apertures," *IEEE Trans. Antennas Propagat.*, vol. 47, pp. 1669–1676, Nov. 1999.

[14] R. F. Harrington, *Field Computation by Moment Methods*. New York: MacMillan, 1968.

[15] R. Tiberio, G. Manara, G. Pelosi, and R. G. Kouyoumjian, "High frequency electromagnetic scattering of plane waves from double wedges," *IEEE Trans. Antennas Propagat.*, vol. 37, pp. 1172–1180, Sept. 1989.

[16] M. Schneider and R. J. Luebbers, "A general uniform double wedge diffraction coefficient," *IEEE Trans. Antennas Propagat.*, vol. 39, pp. 8–14, Jan. 1991.

[17] J. R. Wait, *Electromagnetic Radiation From Cylindrical Structures—Electromagnetic Waves Series*. London, U.K.: IEE Press, 1988, vol. 27.

Hong D. Cheung was born in Taiwan. He received the B.Sc. degree in physics from York University, ON, Canada, in 1994 and the Ph.D. degree in electrical and computer engineering from the University of British Columbia, Vancouver, Canada, in 1999.

Currently, he works in the Electrical and Computer Engineering Department, University of British Columbia, as a Research Assistant. His research interests include the complex source-point method and high-frequency wave propagation and diffraction theory.

Edward V. Jull (M'56–SM'76–F'89–LF'97) was born in Calgary, Canada. He received the B.Sc. degree in engineering physics from Queen's University, Kingston, Canada, in 1956, the Ph.D. degree in electrical engineering from University College, London, U.K., in 1960, and the D.Sc. (Eng.) degree from the University of London, U.K., in 1979.

He was with the Division of Radio and Electrical Engineering of the National Research Council, Ottawa, Canada, from 1961 to 1972. He is now a Professor in the Department of Electrical and Computer Engineering of University of British Columbia, Vancouver. He is the author of *Aperture Antenna and Diffraction Theory*. His research interests include aperture antenna and diffraction theory.

Dr. Jull is was President of International Union of Radio Science (URSI) from 1990 to 1993.